

## MAPPING THE MECHANICAL PROPERTIES OF ALLOYED MAGNESIUM (AZ 61)

Jennifer L. Hay<sup>1</sup>, Phillip Agee<sup>2</sup>

<sup>1</sup>Agilent Technologies; 105 Meco Lane, Suite 200, Oak Ridge, TN 37830

<sup>2</sup>Agilent Technologies; 4330 West Chandler Blvd, Chandler, AZ 85226

Keywords: AZ 61, indentation, hardness, elastic modulus, mechanical-properties map, mesophase

### Abstract

In this work, an advanced form of nanoindentation is used to map the mechanical properties of AZ 61. The probed area includes both alpha (Mg-rich) and beta ( $\text{Al}_{12}\text{Mg}_{17}$ ) phases. The measured moduli of the two phases compare well with expected values. The hardness of the beta phase is three times greater than that of the alpha phase. The hardness map reveals an area of intermediate hardness surrounding the beta phase. This zone is a mesophase which is chemically distinct and may influence the mechanical behavior of the alloy in unexpected ways.

### Introduction

Behind iron and aluminum, magnesium (Mg) is the third most common element used in engineered structures, because it is light-weight, stiff, and strong [1]. Alloying with aluminum can further improve stiffness and strength, although bulk mechanical properties depend strongly on chemical composition and thermo-mechanical history, insofar as these parameters affect microstructure. In this work, we use nanoindentation to determine the properties of individual phases within a popular magnesium alloy, AZ 61.

AZ 61 is a commercially available magnesium alloy which includes aluminum (nominally 6%), zinc (nominally 1%), and other trace elements. Table I provides the chemical composition for AZ 61[2]. The zinc and other trace elements have little effect on microstructure, and the Mg-Al phase diagram is employed to predict the constitution of slowly-cooled AZ 61. At 6% Al, the Mg-Al phase diagram predicts the interaction of two phases: an  $\alpha$  phase which is Mg-rich and a  $\beta$  phase comprising the intermetallic compound  $\text{Al}_{12}\text{Mg}_{17}$ . As the alloy cools from the liquid state, the  $\alpha$  phase begins to solidify at about 620C. Solidification is complete at about 540C, and at this temperature, the material exists entirely in the  $\alpha$  phase. Beginning around 300C, the  $\beta$  phase begins to precipitate and the mass fraction of this secondary phase continues to grow as the material continues to cool. At temperatures below 100C, the  $\beta$  phase accounts for about 7.5% of the material[3].

In this work, we used nanoindentation to measure the elastic modulus and hardness of both phases of AZ 61. Our expectation is that the modulus for each phase should be close to that for the primary component. The primary component of the  $\alpha$  phase is Mg, which has an elastic modulus of 45GPa[1]; however, it should be remembered that at room temperature, the  $\alpha$  phase does include 3% of interstitial aluminum (by mass). Thus, we should not be surprised if the modulus of the  $\alpha$  phase is slightly higher than 45GPa. Zhang et al. calculated the elastic modulus of the

$\text{Al}_{12}\text{Mg}_{17}$  to be 78GPa from first principles[4], so this value sets our expectations for the  $\beta$  phase of AZ 61.

In this work, we used an advanced form of nanoindentation called “Express Test” which performs one complete indentation cycle per second, including approach, contact detection, load, unload, and movement to the next indentation site[5]. This technology enabled us to quantitatively “map” both the elastic modulus ( $E$ ) and the hardness ( $H$ ) of a surface in a reasonable time. This feature is particularly beneficial for probing multi-phase metals such as AZ 61.

Table I. Chemical Composition of Magnesium AZ 61 Alloy [2].

Element	% by mass
Aluminum	5-7
Zinc	0.8-1
Copper	< 0.03
Silicon	< 0.01
Iron	< 0.01
Nickel	<0.005
Magnesium	Balance

### Experimental Method

The sample of AZ 61 tested in this work was prepared by researchers at the Material Science and Engineering Department at Drexel University. AZ 61 chunks were purchased from Thixomat (Livonia, MI). The chunks were placed in alumina crucibles which were covered with alumina disks. Then the crucibles were placed in a vacuum furnace and were heated with a rate of 10°C/min up to 750°C and held for one hour at the temperature after which the furnace was turned off and the samples were furnace cooled. To polish the surface, a section was cut from the sample, mounted, and rough ground with water using silicon carbide, beginning with 400-grit and finishing with 1200-grit (US). The samples were polished using 6 $\mu\text{m}$  and 1 $\mu\text{m}$  diamond on a medium nap cloth with an alcohol-based extender. Scanning electron microscopy was performed with the Agilent 8500 Field Emission Scanning Electron Microscope (Chandler, AZ). The prepared sample was fixed to an SEM stub with carbon tape and mounted onto the SEM sample stage. Imaging was performed with the slowest scan speed, in backscattered electron

mode, with an accelerating voltage of 1kV. The working distance was 2.2mm.

All indentation testing was performed with an Agilent G200 NanoIndenter (Chandler, AZ) having Express Test, NanoVision, and a DCM II fitted with a Berkovich indenter. The test method “Express Test to a Force” was used to perform an array of 20x20 indents within a 50 $\mu$ m x 50 $\mu$ m area; thus, the separation between successive indents was about 2.5  $\mu$ m (2500nm). The peak force for every indent was 4mN; in the  $\alpha$  phase, this force produced a peak displacement of about 380nm; in the  $\beta$  phase, this force produced a peak displacement of about 240nm.

‘Express Test’ is the trade name for a specific option for the Agilent G200 NanoIndenter that allows rapid indentation. Although indents are performed rapidly (one per second), Young’s modulus and hardness are obtained by analyzing the force-displacement data for each indentation according to established norms. These calculations are described in detail elsewhere [6, 7]. Thus, these same measurements could be made by any commercially available instrument that conforms to ASTM E 2546-07 [8] or ISO 14577 [9-11], although the required time would be much longer (on the order of hours, rather than minutes). To perform this work with another instrumented indentation system, the user would simply prescribe a similar array of 20x20 indents, each performed to a peak force of 4mN, all within a 50 $\mu$ m x 50 $\mu$ m area.

## Results and Discussion

The scanning-electron microscopic (SEM) image of Figure 1 shows the microstructure of the AZ 61 surface as prepared for indentation. The  $\alpha$  phase is darker and the precipitated  $\beta$  phase is lighter. From this image alone, one deduces that the  $\beta$  phase is harder, because scratches that span both phases are smaller in the  $\beta$  phase.

Figure 2 shows the maps of elastic modulus ( $E$ ) and hardness ( $H$ ) generated by a 20x20 array of indentations. The total testing time is 15 minutes. Each indentation generates the information content for one pixel; thus, the images in Figure 2 are 400-pixel (20x20) images. The two phases are clearly distinguished. In order to calculate the properties of each phase independently, two rectangular domains were selected which were clearly in either one phase or the other. These are the black and white rectangles in Figure 2.

The black rectangle is in the primary  $\alpha$  phase, which is the Mg with interstitial Al that constitutes about 92% of the material. Within the area bound by the black rectangle, there are 25 indentations; the average elastic modulus for these indentations is  $E = 54.9 \pm 3.3$  GPa, which is slightly higher than the modulus of pure Mg (45GPa) [1]. The average hardness is  $H = 1.35 \pm 0.05$  GPa.

The white rectangle is in the  $\beta$  phase, which is primarily  $Al_{12}Mg_{17}$ . Within the area bound by the white rectangle, there are 15 indentations; the average elastic modulus for these indentations is  $75.8 \pm 3.3$  GPa, which is consistent with the value predicted by Zhang (78GPa)[4]. The average hardness is

$4.3 \pm 0.19$ , which is about three times greater than the hardness of the  $\alpha$  phase. Table II summarizes the properties for each phase.

Surprisingly, the hardness image reveals a region around the  $\beta$  phase in which the hardness is lower than that of the  $\beta$  phase, but higher than that of the  $\alpha$  phase. There are two reasonable explanations for this observation. First, the elevated hardness of the material surrounding the  $\beta$  phase may be caused by (and reveal)  $\beta$  material immediately below the exposed surface. However, modulus is usually more sensitive to the influence of constraining material, and the modulus is uniform outside the  $\beta$  phase. It must be granted, however, that the difference in hardness between the two phases is much greater than the difference in modulus, so the hardness may manifest more constraint effect than modulus simply because there is a greater difference in hardness between the two phases.

The second (and more interesting) explanation is that the material around the  $\beta$  phase may be a true “mesophase” if it is chemically different than either  $\alpha$  or  $\beta$ . More detailed analysis of the chemistry and microstructure of this region by means of energy dispersive x-ray spectroscopy (EDX), transmission electron spectroscopy (TEM), and focused-ion beam milling (FIB) may shed more light on this phenomenon.

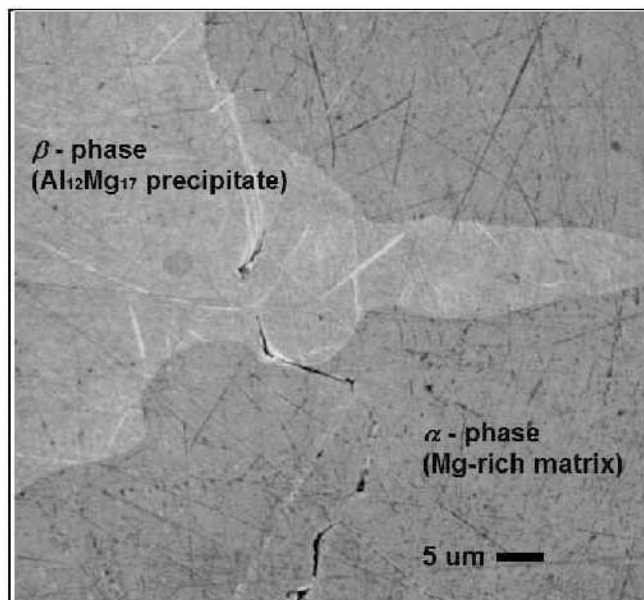


Figure 1. Low-voltage, field-emission, scanning-electron-microscopy image of Mg AZ 61 as prepared for nanoindentation. Acquired in back-scattered electron (BSE) mode. Image resolution is 1024x1024 pixels. Smaller scratches in the  $\beta$  phase evidence higher hardness.

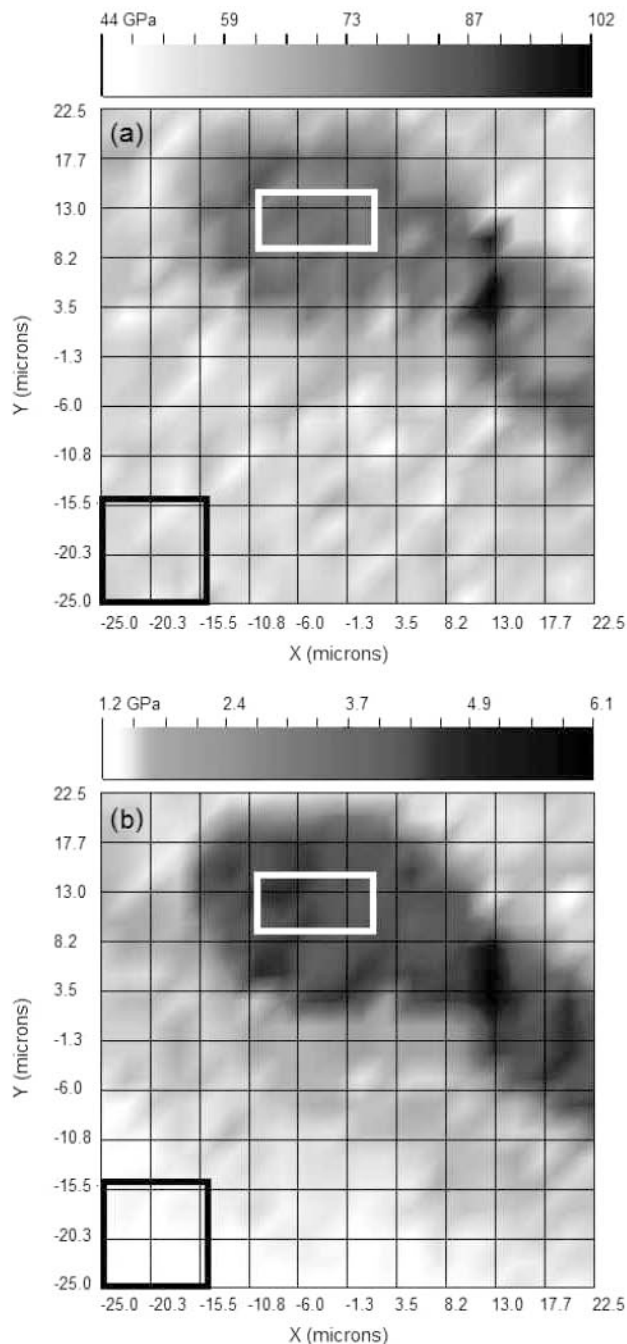


Figure 2. (a) Modulus and (b) hardness of two-phase Mg AZ 61. Black rectangles are in the primary  $\alpha$  phase (Mg-rich). White rectangles are in the  $\beta$  phase ( $\text{Al}_{12}\text{Mg}_{17}$ ). Information for both images was acquired in 15 minutes by means of the Express Test option for the Agilent G200 NanoIndenter (Chandler, AZ). Image resolution is 20x20 pixels.

Table II. Properties of Magnesium AZ 61 Constituents Measured by Nanoindentation at 4mN

Material	N	$E$ GPa	$H$ GPa
$\alpha$ -phase (Mg-rich)	25	$54.9 \pm 3.3$	$1.35 \pm 0.05$
$\beta$ -phase ( $\text{Al}_{12}\text{Mg}_{17}$ )	15	$75.8 \pm 3.3$	$4.30 \pm 0.19$

<sup>1</sup>c.f. the modulus of pure Mg (45GPa) [1]

<sup>2</sup>c.f. the modulus of  $\text{Al}_{12}\text{Mg}_{17}$  calculated by Zhang et al (78GPa) [4]

### Conclusions

In this work, the Express Test option for the Agilent G200 NanoIndenter was used to map out the mechanical properties of a magnesium alloy, AZ 61. The measured moduli of the  $\alpha$  and  $\beta$  phases compared well with expected values. The hardness of the precipitate ( $\beta$ ) phase was three times greater than that of the  $\alpha$  phase. The hardness map revealed an area of intermediate hardness surrounding the  $\beta$  phase; more analysis is required to fully explain this phenomenon.

### Acknowledgements

The authors gratefully acknowledge Dr. Hamdallah Bearat of Arizona State University for the SEM images. The authors further acknowledge Mr. Babak Anasori and Dr. Michel Barsoux of the Materials Science and Engineering Department of Drexel University for providing the sample of AZ 61 tested in this work.

### References

1. "Magnesium," [Date Accessed: July 9, 2012] Available from: <http://en.wikipedia.org/wiki/Magnesium>.
2. C.-F. Fang, X.-G. Zhang, S.-H. Ji, J.-Z. Jin, and Y.-B. Chang, "Microstructure and corrosion property of AZ61 magnesium alloy by electromagnetic stirring," *Trans. Non Ferrous Met. Soc. China*, 15 (3) (2005), 536-541.
3. James F. Shackelford, *Introduction to Materials Science for Engineers, Second Edition* (New York, NY: Macmillan Publishing Company, 1988), 223.
4. H. Zhang et al., "First-principles calculations of the elastic, phonon and thermodynamic properties of  $\text{Al}_{12}\text{Mg}_{17}$ ," *Acta Materialia*, 58 (2010), 4012-4018.
5. J.L. Hay, "Revolutionary New Agilent Express Test Option for G200 NanoIndenters," [Date Accessed: April 9, 2012] Available from: <http://cp.literature.agilent.com/litweb/pdf/5990-9948EN.pdf>.
6. W.C. Oliver and G.M. Pharr, "An Improved Technique for Determining Hardness and Elastic Modulus Using Load and

Displacement Sensing Indentation Experiments,” *Journal of Materials Research*, 7 (6) (1992), 1564-1583.

7. J.L. Hay, “Introduction to Instrumented Indentation Testing,” *Experimental Techniques*, 33 (6) (2009), 66-72.
8. ASTM E2546-07, “Standard Practice for Instrumented Indentation Testing,” (2007), Available from: <http://www.astm.org/Standards/E2546.htm>.
9. ISO 14577-1:2002, “Metallic Materials—Instrumented Indentation Test for Hardness and Material Parameters—Part 1: Test Method,” (2002), Available from: <http://www.iso.org>.
10. ISO 14577-2:2002, “Metallic Materials—Instrumented Indentation Test for Hardness and Material Parameters—Part 2: Verification and Calibration of Testing Machines,” (2002), Available from: <http://www.iso.org>.
11. ISO 14577-3:2002, “Metallic Materials—Instrumented Indentation Test for Hardness and Material Parameters—Part 3: Calibration of Reference Blocks,” (2002), Available from: <http://www.iso.org>.